Next Materials 12 (2026) 102045

Contents lists available at ScienceDirect

Next Materials

journal homepage: www.sciencedirect.com/journal/next-materials

Research article

Harnessing *Euphorbia wallichii* for the sustainable synthesis of $CoFe_2O_4$ nanoparticles with photocatalytic and antibacterial potential

Sabeeha Jabeen [a,1], Sana Nisar [a,1], Vasi Uddin Siddiqui [b], Shumaila Suhail [a], Arshad Iqbal [c], Naseem Ahmad [a], Nafees Ahmad [a,*]

[a] Department of Chemistry, Integral University, Lucknow, Uttar Pradesh 226026, India
[b] Advanced Engineering Materials and Composites Research Centre (AEMC), Department of Mechanical and Manufacturing Engineering, Universiti Putra Malaysia, UPM, Serdang 43400, Malaysia
[c] Department of Physics, Integral University, Lucknow, Uttar Pradesh 226026, India

ARTICLE INFO

Keywords:
Biosynthesis
Phyto-functionalized $CoFe_2O_4$ NPs
Euphorbia wallichii
Photocatalysis
Antibacterial activity
Electrochemical activity

ABSTRACT

The present study addresses the bio-mediated synthesis of phyto-functionalized cobalt ferrite nanoparticles ($CoFe_2O_4$ NPs) by means of *Euphorbia wallichii* leaf extract, which deals a green and sustainable route for the synthesis of nanoparticles. The leaf extract acts as a reducing and stabilizing agent in the synthesis of $CoFe_2O_4$ NPs. The characterizations of $CoFe_2O_4$ NPs were carried out using X-ray diffraction (XRD) to confirm the phase and crystallinity, elemental composition and morphology were checked using scanning electron microscope coupled with energy dispersive spectroscopy (SEM-EDX). FTIR spectroscopy was used for functional groups analysis, and UV-DRS to calculate the bandgap energy. Moreover, the electrochemical surface area of $CoFe_2O_4$ was determined by a potentiostat using Cyclic Votammetry (CV) technique. The phyto-functionalized $CoFe_2O_4$ NPs showed excellent photocatalytic activity and 94.7% methylene Blue (MB) dye was degraded in 90 min under visible light irradiation with the rate constant 0.07935 min^{-1}. Further, trapping and recycling experiments were also carried out to check the durability of the photocatalyst, and the results indicate that the degradation efficney of $CoFe_2O_4$ NPs was only decrease by 2.4%, even after four consecutive cycles. Moreover, the $CoFe_2O_4$ NPs exhibited potent antibacterial activity towards Gram-positive and Gram negative bacterias, highlighting the property of $CoFe_2O_4$ NPs for environmental and biomedical applications.

1. Introduction

In recernts years, nano-sized spinal ferrites have attracted much attention due to their remarkable properties such as higher surface area, chemical and thermal stability and magnetic properties etc. Amiri et al., [1,2]. The spinel ferrite (AB_2O_4) such as $MgFe_2O_4$, $MnFe_2O_4$, $CoFe_2O_4$, $CuFe_2O_4$, etc are used in biomedicine, energy, coloring, sensors and for environmental remediation [3,4]. Recently, these spinal ferrites are used as photocatalysts for the removal of wide range of micropollutants i.e. fertilizers, toxic dyes, pharmaceutical products and polyaromatic hydrocarbons through the photocatalysis method [5,6]. Photocatalytic process is much efficient, less time consuming and cost effective process as compared to other processes i.e physical and biological methods for micropollutant removal ([7–9],). The spinel ferrites are prepared through various routes i.e. sol–gel auto combustion, ball milling, hydrothermal decompositions, co-precipitation and micro-emulsion methods [10]. However, spinel ferrite can also be synthesised by green approach using various plant extract due to its efficient and cost effective nature which also reduces the environmental burden [11]. The green synthesis approach of the nanoparticle utilizes plant extract such as leaves, roots, and seeds, agricultural and biological wastes as eco-friendly nontoxic precursors. Various extract that are commonly used for the synthesis of nanoparticles are extract of Hibiscusrosa-sinesis, Aloe vera, sesame seeds, turmeric, ginger roots etc. These extract contains various organic and inorganic phytochemicals capable of reducing the metal nitrates to the metal NPs. Therefore, the reaction between metal nitrates and plant extract becomes efficient because of the uniform distribution of biological molecules and high solubility [12]. Moreover, plant extracts which contains phytochemicals (polysaccharides, phenolic acids, flavonoids, etc.) are used for reducing, chelating,

* Corresponding author.
E-mail addresses: anafees@iul.ac.in, Siddiquenafees123@gmail.com (N. Ahmad).
[1] These authors have contributed equally to this work.

https://doi.org/10.1016/j.nxmate.2026.102045
Received 5 January 2026; Received in revised form 15 March 2026; Accepted 6 April 2026
Available online 13 April 2026

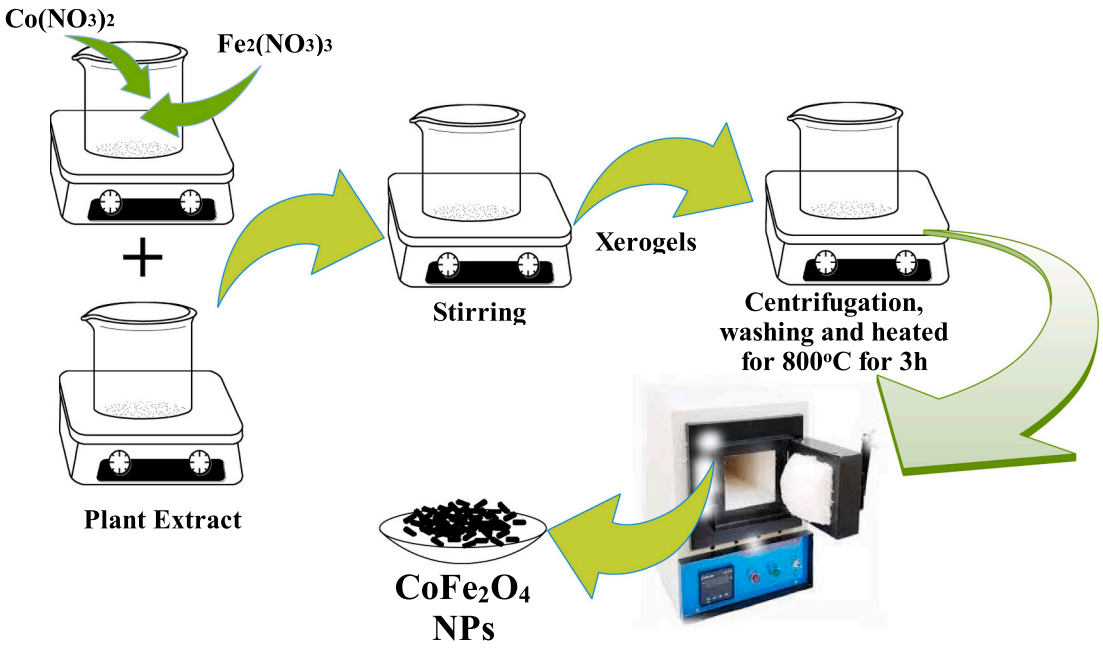

Fig. 1. Overview for the fabrication of $CoFe_2O_4$ NPs.

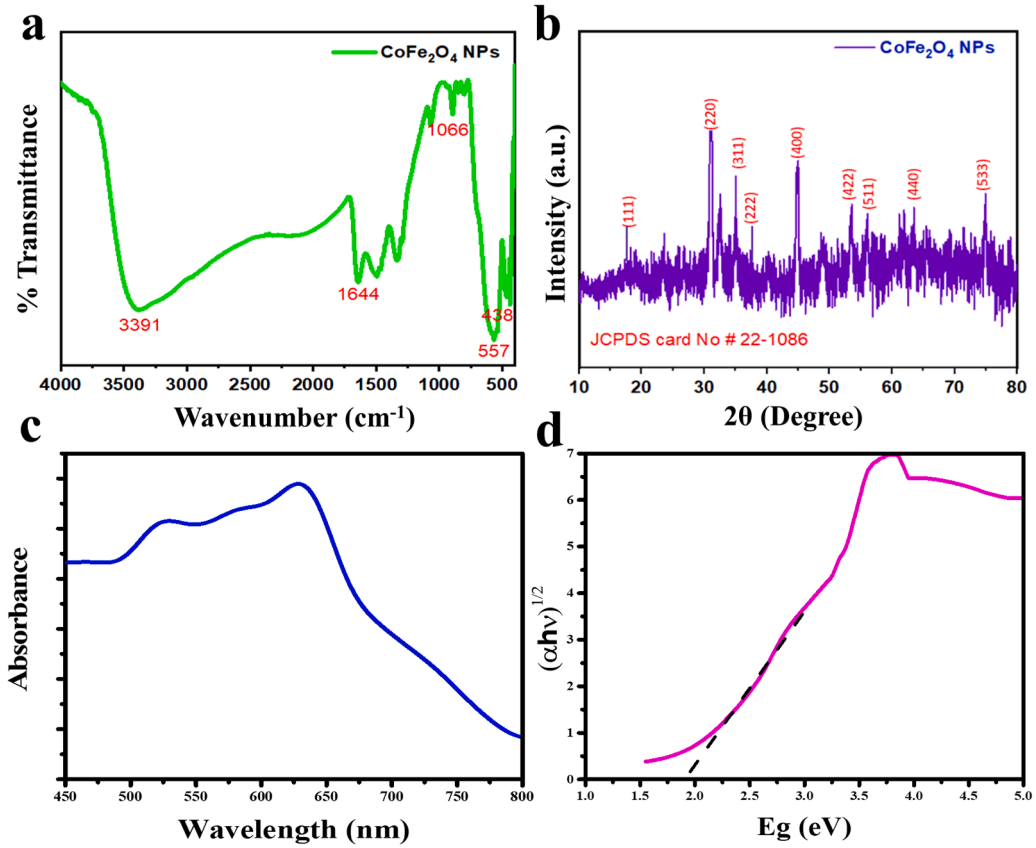

Fig. 2. (a) FTIR spectrum (b) XRD spectrum of synthesized $CoFe_2O_4$ NPs (c) UV-Visible spectra and (d) TauC plot of $CoFe_2O_4$ nanoparticle.

stabilizing and capping agents in the synthesis of nanomaterials [13]. The variations in concentrations of these active phytochemicals, and their interactions through metal ions are key aspects that contribute to the uniformirty of shapes and size of the resulting nanoparticles. During the synthesis process, biological molecules from the plant extracts become immobilized on the surfaces of the nanoparticles, leading to the functionalization or coating of these surfaces, which enhances the stability of the biosynthesized nanoparticles.

Among the various spinal ferrite nanoparticles, cobalt ferrite ($CoFe_2O_4$) has gained specicial significance due to its high coreactivity, good chemical stability and moderate magnetization [14]. Cobalt ferrite has also received much attention towards reserachers due to its wide

Table 1
Calculation of the average size of synthesized $CoFe_2O_4$ NPs.

S. No	K	λ (Å)	Peak position 2θ (°)	FWHM Beta size (°)	D (nm)
1	0.94	1.54178	18.9°	.45634	18.447
2	0.94	1.54178	30.40°	.44371	19.393
3	0.94	1.54178	35.22°	.44101	19.755
4	0.94	1.54178	37.1°	.41576	21.067
5	0.94	1.54178	43.2°	.50753	17.597
6	0.94	1.54178	53.12°	.51446	18.045
7	0.94	1.54178	56.28°	.55324	17.021
8	0.94	1.54178	62.33°	.64437	15.06
9	0.94	1.54178	75.32°	.64513	16.259
Average crystallite size				**19.74 nm**	

range of applications towards biomedical and environmental applications [15,16]. For the last few years, various studies have been reported for the bio-mediated synthesis of cobalt ferrite using different plant extract. For example, [17] utilized Aloe vera in a sol–gel auto–combustion method for the synthesis of $CoFe_2O_4$ NPs for high-frequency magneto recording devise. In another study, [18] described the synthesis of $CoFe_2O_4$ using tulsi seed, which exhibited excellent antibacterial activity. [19] used extracts from the hairy roots of Artemisia annua L. to the sustainable synthesis of $CoFe_2O_4$ NPs and recorded the effects and roles of green route parameters.

In the present study, $CoFe_2O_4$ nanoparticles was synthesized using *Euphorbia wallichii* extract. *Euphorbia wallichii* is among the largest genera of flowering plants and third-largest angiosperm genus. *Euphorbia wallichii* contains important secondary metabolites, including diterpenoids and triterpenoids, that was used in the treatment of many diseases [20]. *Euphorbia wallichii* contains diterpenoids and flavonoid which provide stronger chelation and capping ability leading to controlled particle size and stability. Futher, the synthesized $CoFe_2O_4$ nanoparticles was used as catalysts for the photodegradation of MB dye and also tested for antibacterial property against *Listeria monocytogenes*, *Staphylococcus aureus*, *Klebsiella pneumonia*, *Pseudomonas aeruginosa* bacteria. Green synthesized $CoFe_2O_4$ nanoparticles demonstrate excellent activity towards the photodegradation of pollutants and antibacterial activity suggesting their dual role for the environmental remediation and biomedical applications.

2. Experimental section

2.1. Material and methods

The *Euphorbia wallichi* leaves were collected from Integral University, Lucknow, India. Iron nitrate nonahydrate $Fe(NO_3)_3.9H_2O$, dimethyl sulphoxide (DMSO) and Cobalt nitrate hexahydrate ($Co(NO_3)_2.6H_2O$) and Methylene Blue were purchased from Sigma Aldrich, India. Distilled water was used as a solvent for all metallic salts. The 2 g-positive and 2 g-negative bacterial strains viz. *Listeria monocytogenes*, *Staphylococcus aureus*, *Klebsiella pneumoniae*, and *Pseudomonas aeruginosa* that are used for antimicrobial analysis were obtained from Microbial Type Culture Collection and Gene Bank Chandigarh, India. The bacterial strains were maintained on nutrient agar medium.

2.2. Preparation of Euphorbia wallichi leaf extract

The fresh leaves were collected and washed with deionized water multiple times and kept in an oven for 30 min to dry. Further, the leaves were chopped into small pieces, grounded to fine powder and boiled in

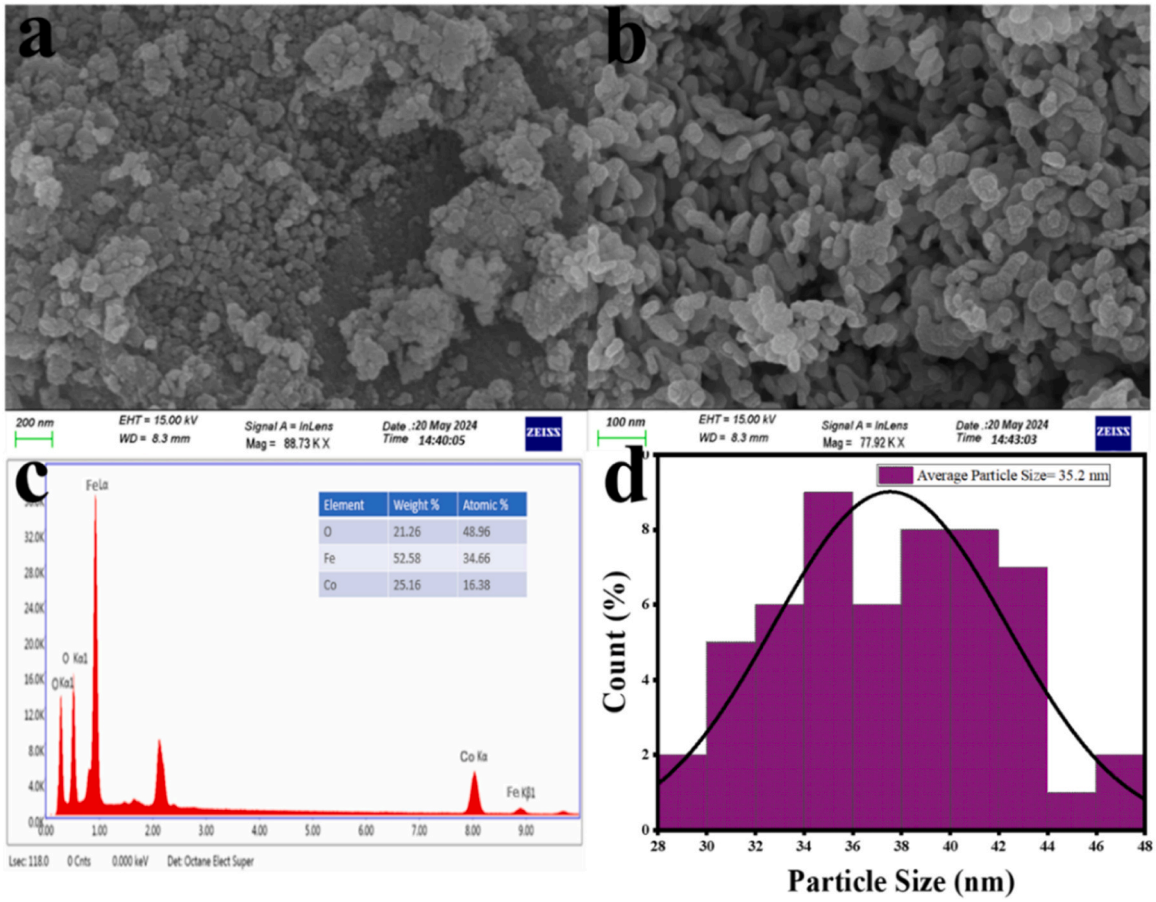

Fig. 3. (a,b) FE-SEM image of $CoFe_2O_4$ at different mangnifications (c) EDS spectra and (d) histogram of particle size distribution of $CoFe_2O_4$ NPs.

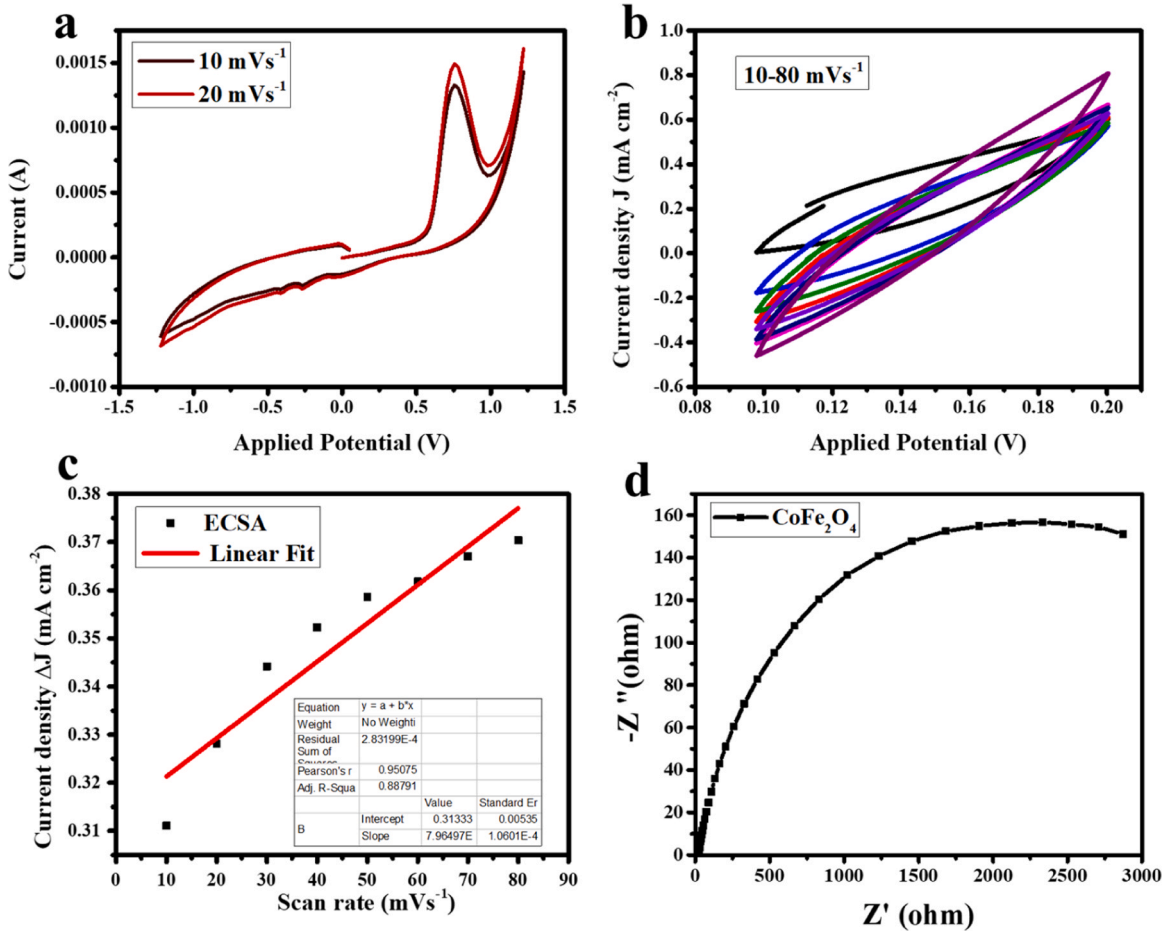

Fig. 4. (a) Cycliv voltammogram at different scan rates (b) EDLC curve (c) the linear fit of the scan rates plot against EDLC (d) Nyquist plot of $CoFe_2O_4$.

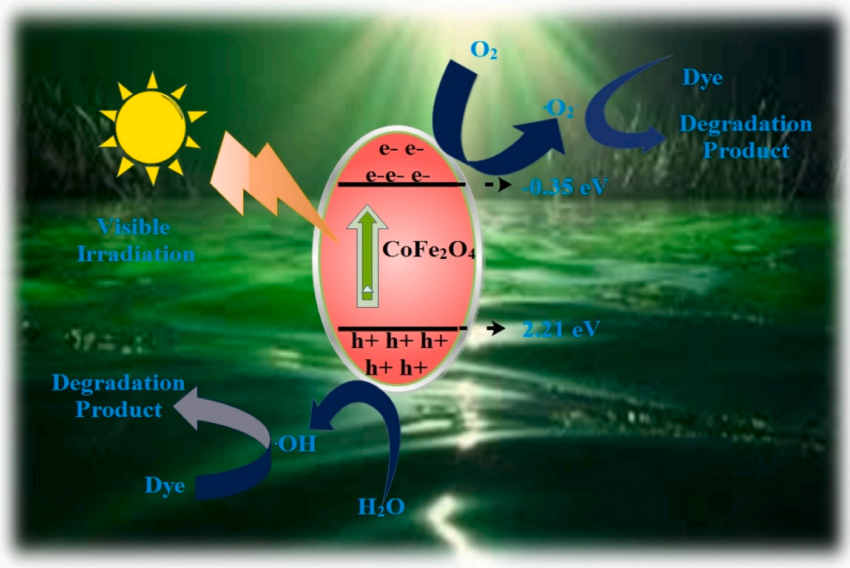

Fig. 5. Probable photocatalytic mechanism for the degradation of MB dye by $CoFe_2O_4$ NPs.

200 ml deionized water at 80°C for 30 min in round bottom flask. After cooling the mixture, the extract is filtered by Whatmann filter paper and kept for drying for further use [21].

2.3. Green fabrication of $CoFe_2O_4$ NPs

For the synthesis of $CoFe_2O_4$ NPs, a separate 0.1 M solution of Co $(NO_3)_2.3H_2O$) and $Fe(NO_3)_3.9H_2O$ were prepared. Further, plant extract (30 ml) was added to the 10 ml each of $Co(NO_3)_2.3H_2O$) and Fe

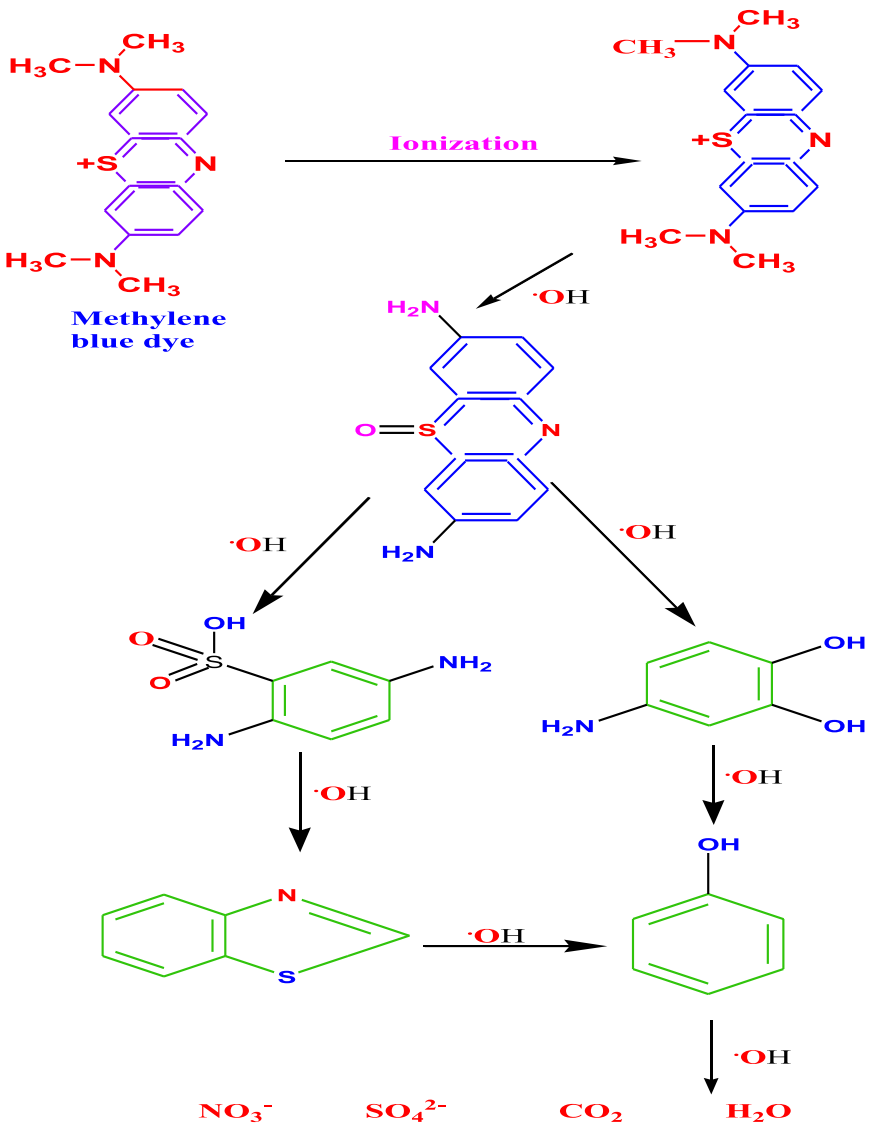

Fig. 6. Proposed degradation pathways of MB dye.

$(NO_3)_3.9H_2O$ and kept for stirring until the solutions are properly homogenized at room temperature. Finally, NaOH solution was added slowly to the solution mixture to maintain the pH value at 8. The mixing process continues on a magnetic stirrer to ensure mix the solution and a good distribution of the components at room temperature. After some time, the temperature was gradually increased and fixed at 90°C, then a dry gel mixture was obtained. This dry gel was heated at 800°C for 3 hrs to obtain crystallized $CoFe_2O_4$ NPs [22]. These $CoFe_2O_4$ NPs were separated by centrifugation at 10,000 rpm for 15 mins and washed by ethanol and water multiple times. Further, the $CoFe_2O_4$ NPs were calcined in a muffle furnace at 400°C for 4 hr to get the final product. An overview of the synthesis of $CoFe_2O_4$ NPs is presented in Fig. 1. The yield obtained from the green route was 89.2% which is higher than that of chemically synthesized $CoFe_2O_4$ (81%) shows that the green route offers improved synthesis efficiency. All the experiments performed was repeated twice in order to confirm the reproducibility of the reactions.

2.4. Antibacterial activity: Media preparation and sterilization methodology

Anticatreioal evaluation of the bio-mediated synthesized $CoFe_2O_4$ NPs was carried out by using Mueller Hinton Agar (HiMedia Laboratories Private Limited) petri plates to grow the culture of bacteria i.e. two gram positive bacteria (*Listeria monocytogenes*, *Staphylococcus aureus*) and 2 g negative bacteria (*Klebsiella pneumoniae*, *Pseudomonas aeruinosa*). In the antibacterial experiment, agar wells (5*5 mm) were filled with the varying concentrations of $CoFe_2O_4$ NPs using DMSO as negative control and getamucin as a positive control. After being sealed and incubated for 24 hrs at 37°C, the Petri plates were checked for the zone of inhibition. The activity was recorded in triplicate.

2.5. Materials characterizations

The phase, crystal lattice of the synthesized $CoFe_2O4$ NPs are confirmed by using a X-ray diffractometer (XRD- Rigaku Ultima IV, Tokyo, Japan) ranges 20° to 80° using monochromatic CuK radiation (λ = 1.54 Å). The UV–visible spectrum was recorded between 200–800 nm using (Hitachi model-U3900, Tokyo, Japan). The morphology and the structure of the sample was studied by FE-SEM microscope (Model No. SIGMA VP, Zeiss, Germany). Moreover, the functional group analysis was carried out by FT-IR spectrometer of Model-Bruker Tensor 37, Billerica, MA, USA) using potassium bromide (KBr) palette.

2.6. Photocatalytic activity study and trapping experiment

The photochemical reactor was used to experiment, fitted with a

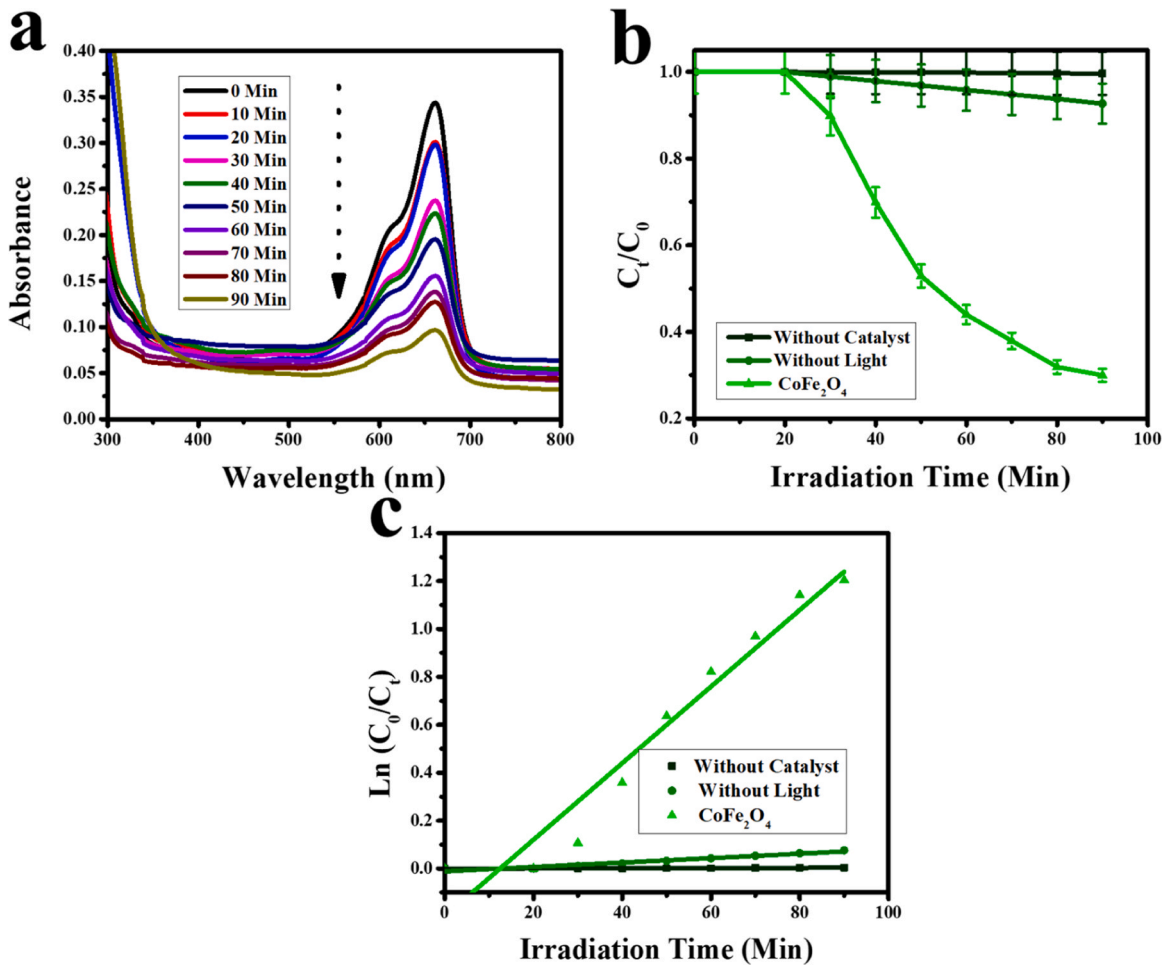

Fig. 7. (a) UV-Visible spectra of the MB dye (b) Kinetics of photodegradation (c) rate constant curve of the $CoFe_2O_4$ and controlled test.

visible lamp of intensity 500 W in the wavelength range of 400–700 nm, for irradiation and an oxygen pump was provided for atmospheric oxygen. An amount of the photocatalyst (0.02 g) was mixed with 100 ml of MB solution prepared in distilled water and placed in the photochemical reactor. Before the irradiation started, the sample was kept in the dark to maintain the adsorption/desorption equilibrium between $CoFe_2O_4$ and the MB dye solution, and after 20 min, 3 ml of the MB dye sample was withdrawn from the reactor at a predetermined time to check the degradation using a UV–visible spectrophotometer. The absorbance of the MB dye sample was checked at $\lambda_{max} = 637$ nm. The degradation efficiency can be calculated by the following formula, as shown in Eq. (1) from the absorbance data.

$$\text{Degradation efficiency} = C_0 - C_t / C_0 * 100 \quad (1)$$

In Eq. (1), C_0 is the initial concentration, and C_t is the concentration after time (t) of the MB dye. Additionally, to ensure the reactive oxygen species (ROS) accountable for the degradation of MB dye, various traping agnets i.e. Isopropyl alcohol, (IPA) to trap $^{\circ}OH$, Na-ethylenediamminetetracetic acid (Na-EDTA) for h^+ and p-benzoquinone to trap $^{\circ}O_2^-$. Further, the durability of the $CoFe_2O_4$ was tested by using recycling experiments by using the $CoFe_2O_4$ nanoparticle for four consecutive cycle.

3. Result and discussion

3.1. Structural and optical analysis

The functional group analysis of $CoFe_2O_4$ nanoparticles was characterized by the FTIR spectroscopy as shown in Fig. 2a. The peaks observed at 3391 cm^{-1} and 1644 cm^{-1} are assigned to OH and H-O-H stretching vibrations. The spectrum also shows two significant absorption bands one at 557 cm^{-1} and 438 cm^{-1} corresponding to Fe-O and Co-O stretching vibrations in the tetrahedral and octahedral coordination sites respectively [2,23].

Further, the phase and crystallinity behavior of the $CoFe_2O_4$ nanoparticle was characterized by XRD as shown in Fig. 2b. The diffraction peaks were found at 2θ values around 18.9°, 30.40°, 35.22°, 37.1°,43.2°, 57.12°, and 62.33° which could be accounting for crystal planes. The XRD pattern displays distinct reflections at (111), (220), (311), (222), (400), (422), (511), (440), and (533) planes, corresponding to face-centered cubic $CoFe_2O_4$ phase [24,25]. The D-spacing is found to be 1.488 Å and lattice parameters for cubic spinel $CoFe_2O_4$ sample is found to be a = b = c = 4.208 Å from the data. The intense and sharp nature of these peaks reveals excellent crystallinity. All characteristic peaks align well with JCPDS 22–1086 standard and no impurity peaks were detected, confirming the material's pure phase [26]. A plane is a major plane with most particles having faced centered cubic (FCC) crystalline structure. Moreover, the crystallite size of $CoFe_2O_4$ nanoparticle was calculated using the scherrer's equation.

$$D = \frac{k\lambda}{\beta Cos\theta} \quad (2)$$

Where K= 0.94 as the shape constant, λ, X-ray wavelength which is 1.542(Å), β representing the full width at half maxima (FWHM) of the peak and θ is the Bragg's angle. The average crystallite size obtained from the XRD pattern is around 19.74 nm, as given in Table 1.

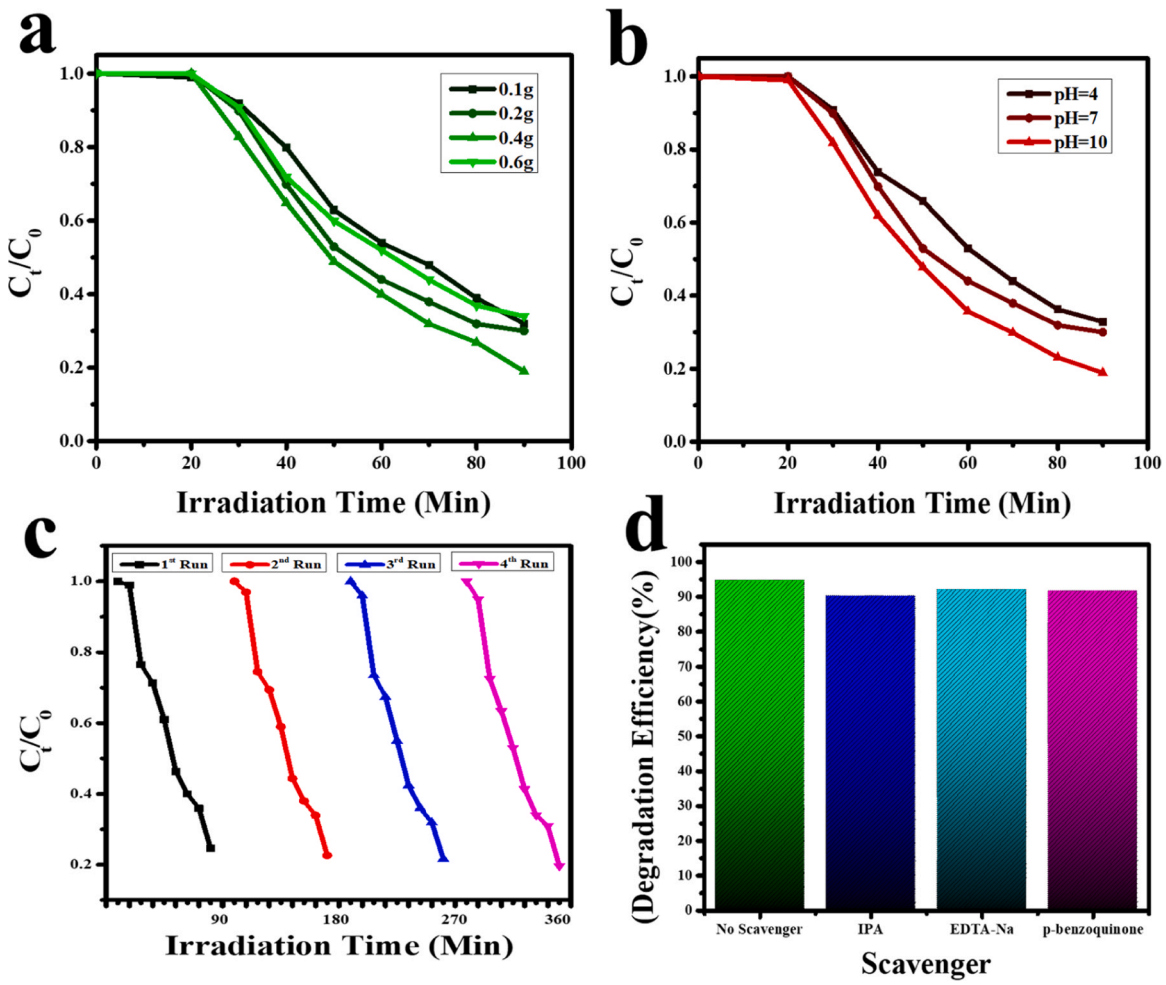

Fig. 8. (a) Effect of catalyst dosage (b) Effect of pH (c) Recycling experiment and (d) is the effect of scavenger on photodegradation.

Further, the band gap energy of the $CoFe_2O_4$ nanoparticles was determined by the UV-DRS spectroscopy using TauC plot. The optical band gap energy was determined from the following equation:

$$h\upsilon.\ \alpha = (Ah\upsilon - E_g)^{n/2} \quad (3)$$

where α represents the absorption coefficient, hυ is the photon energy, and E_g corresponds to the band gap energy and the value of n = 1 was used for the indirect transition. In the Fig. 2c, an absorption band is shown at 637 nm, and the band gap energy was calculated from the TauC plot, which is 1.96 eV as shown in Fig. 2d which is inaccordance to previous reported literature [27].

3.2. Morphological studies

The morphological studies of $CoFe_2O_4$ nanoparticle was carried out by FE-SEM coupled with EDX. The FE-SEM images with different magnification in shown in Fig. 3(a,b). The uniform size of the granular coral-like morphology of $CoFe_2O_4$ nanoparticle can be seen from Fig. 3a, b. Further, EDX study indicates the presence of Co, Fe and O as shown in Fig. 3c [28]. The average particle size of the $CoFe_2O_4$ nanoparticle was calculated by the imagej software and found to be 35.2 nm. The histogram for the particles size distribution is presented in Fig. 3d.

3.3. Determination of electrochemical surface area

The cyclic voltammetry method was used to determine the electrochemical surface area (ECSA) of biosynthesised $CoFe_2O_4$ NPs. Measurements work carried out using these three electrode setups in the potential widow of −1.5 to + 1.5 V. The Ag/AgCl electrode served as the reference electrode (0.193 mV, 3 M of Cl). The working electrode was a glassy electrode (GCE), the counter electrode was platinum (Pt) wire, and the electrolyte was a 0.1 M KOH solution. The sample was nitrogen-purged to preserve the inert environment before analysis. The $CoFe_2O_4$ NPs (0.2 mg) were immobilized on the glassy carbon electrode surface, where nafion used as a binder for proper attachment. The cyclic voltammograms were achieved at various scan rates of 10 mVs^{-1} and 20 mVs^{-1} within a potential window of −1.5 to + 1.5 V as illustrated in Fig4a. The cyclic voltammograms were used to determine the electro double layer capacitance (EDLC) at various scan rates in the range of 10–80 mVs^{-1} presented in Fig. 4b. The value of the slope of the EDLC plot against various scan rates ranging from 10 to 80 mVs^{-1} was used to evaluate ECSA, which was found to be 00159 $mFcm^{-1}$ as shown in Fig. 4c [29,30]. A higher ECSA endorses the generation of reactive oxygen species (ROS) i.e. $^{\circ}OH$ and $^{\circ}O_2^-$ and these ROS helps in the photodegradation of dyes and damage the bacterial cell walls, proties and DNA leading to cell death. Additionally, EIS study was carried out the check the charge transfer resistance which shows the electrical conductivity and interfacial charge transfer behavior of the $CoFe_2O_4$ indicated by the diameter of the semicircle. The Nyquist plot of $CoFe_2O_4$ presented in Fig. 4d shows very small diameter corresponds to faster electron transfer kinetics and redox activity [31].

3.4. Photocatalytic degradation of dye and mechanistic approach

The photocatalytic mechanism of the $CoFe_2O_4$ NPs is based on the

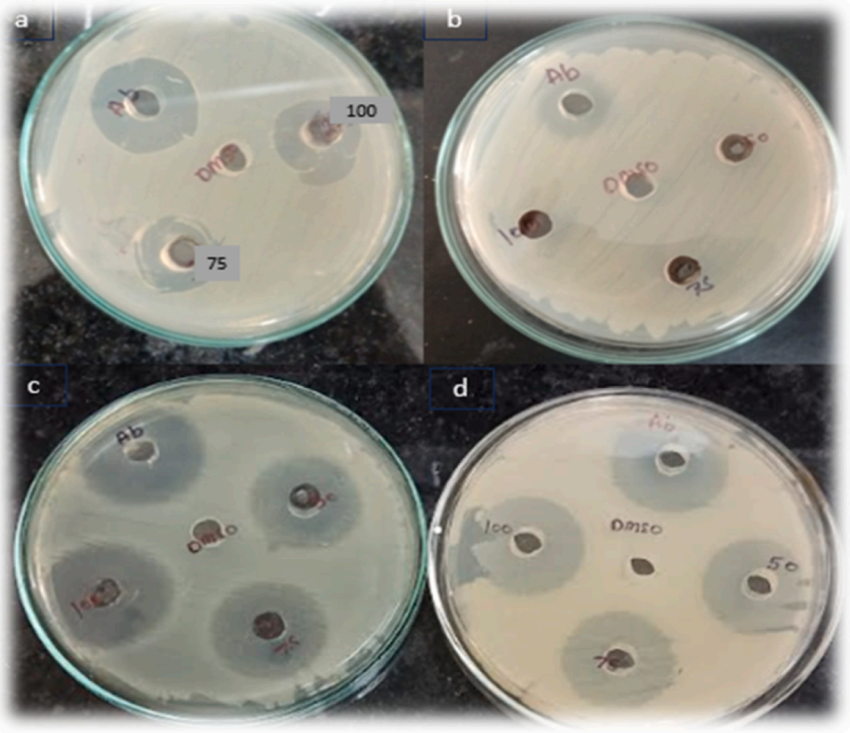

Fig. 9. Antibacterial activity of $CoFe_2O_4$ NPs against (a) Listeria monocytogenes (b) Staphylococcus aureus (c) Klebsiella pneumonia (d) Pseudomonas aeruginosa.

Table 2
Zone of inhibition (mm) of the synthesized $CoFe_2O_4$ NPs.

S. No.	Bacterial strain	Zone of Inhibition (mm) In different conc. (mg/ml L) of $CoFe_2O_4$ NPs			Gentamycin (Standard) (mm)	Control (DMSO)
		50	75	100	50 mg/ml	
1	*Listeria monocytogenes*	-	15 ± 0.6	17 ± 0.8	20 ± 0.2	0.0
2	*Staphylococcus aureus*	0.1 ± 0.2	0.1 ± 0.3	0.1 ± 0.4	0.5 ± 0.1	0.0
3	*Klebsiella pneumoniae*	15 ± 0.2	18 ± 0.2	21 ± 0.4	21 ± 0.2	0.0
4	*Pseudomonas aeruginosa*	18 ± 0.2	19 ± 0.6	20 ± 0.3	20 ± 0.1	0.0

potentials of conduction band and valence band in the order to determine the pathways of the mechanism. The potential of the valence band edge (E_{VB}) and conduction band edge (E_{CB}) was estimated using Eq. 4:

$$E_{VB} = X - E^e + 0.5\ E_g \quad (4)$$

Where X represents electronegativity of the atoms, E_g is the optical bandgap energy. E^c is the free electron energy. Subsequently, the conduction band potential (E_{CB}) was calculated from Eq. 5:

$$E_{CB} = E_{VB} - E_g \quad (5)$$

The potential of the valence band and conduction band of $CoFe_2O_4$ NPs was calculated from the above Eqs. (4, 5) and found to be 2.21 eV and −0.35 eV respectively. In Fig. 5, the detailed photocatalytic mechanism for the degradation of MB dye is presented. Upon the irradiation of photons of suitable wavelength to $CoFe_2O_4$ nanoparticles, molecular excitation occurs, resulting in generation of photo induced charge carriers (e^-/h^+) [32–34]. The photo induced electrons in the conduction band of $CoFe_2O_4$ nanoparticle surface interact with the molecular O_2 to produce superoxide anions radicals ($^\circ O_2^-$). In the mean time, the photogenerated holes in the valence band (h^+) reacts to the H_2O molecules to form hydroxyl radical ($^\circ OH$). These superoxide anions radicals and hydroxyl radical generated in the mechanistic pathways reacts to the MB molecule leads to the mineralization.

Form the above mechanism, the photocatalytic reactions involve in the degradation of MB dye molecule can be described as:

$$CoFe_2O_4 + h\nu \rightarrow CoFe_2O_4\ (e^-_{CB} + h^+_{VB}) \quad (6)$$

$$e^-_{CB} + O_2 \rightarrow {}^\circ O_2^- + H^+ \rightarrow HOO^\circ \quad (7)$$

$$h^+_{VB} + H_2O \rightarrow {}^\circ OH + H^+ \quad (8)$$

Reactive oxygen species ($^\circ OH$, $^\circ O_2^-$) + MB dye → Decomposed products (9)

Therefore, the generation of highly active oxygen radicals ($^\circ O_2^-$ and $^\circ OH$) plays a crucial role in breaking down the dye molecule into harmless product. The degradation product of the MB dye is shown below Fig. 6.

The UV–visible spectra of the degraded samples of MB dye are shown in Fig. 7a. The gradual decrease in the absorbance shows the degradation of the MB dye. Based on the results obtained from the UV–visible spectra, the photocatalytic degradation kinetics was studied and the rate constant was calculated using Langmuir Hinshelwood Eqs. (10, 11):

$$C_t/C_0 = e\hat{}(-kt) \quad (10)$$

$$\ln\ [C_t/C_0] = -kt \quad (11)$$

From the equations, the rate constant of $CoFe_2O_4$ NPs was calculated using the plot between MB concentration and time, which follows the first-order kinetics of degradation as shown in Fig. 7b. The rate constants were determined to be 0.00031 min^{-1} for the control reaction (without catalyst), 0.001231 min^{-1} (without light) and 0.07935 min^{-1} for the $CoFe_2O_4$ nanoparticle. A comparative table (Table S1) of photocatalytic performance of the previously reported $CoFe_2O_4$ nanoparticles have been provided supplementary information. Further, in accordance to the

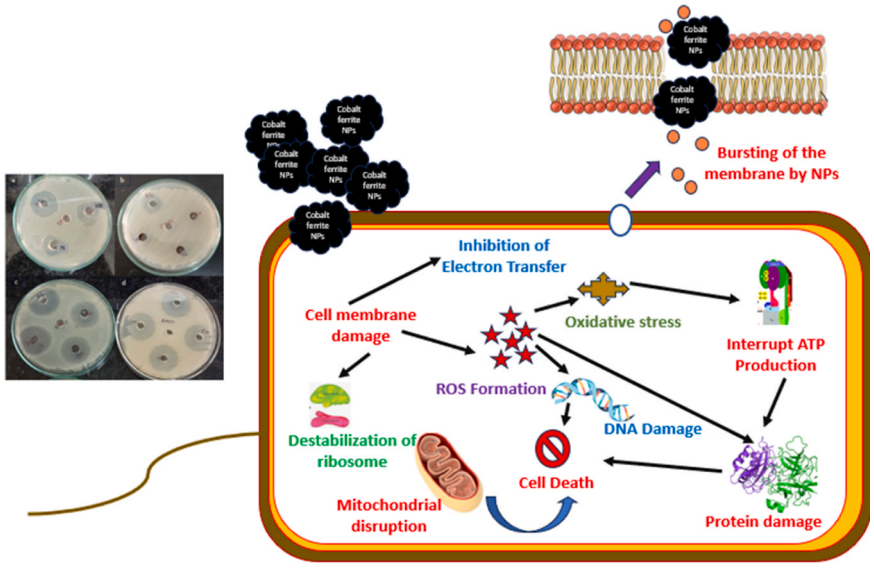

Fig. 10. Probable mechanism involved in antibacterial activity of $CoFe_2O_4$ NPs.

rate constant values obtained from the the data, rate constnt curve are plotted as shown in Fig. 7c.

The effect of pH was studied by maintain the aqueous solution at pH 4, 7 and 10 by adding NaOH and HCl. The higher degradation was observed in basic medium at pH 10 which is due to the formation of OH^- ions in the solution (Fig. 8a). These OH^- ions traps the photogenerated holes (h^+) in the solution and form °OH radicals [35]. These °OH radicals are the prime species for the degradation of methylene blue dye. Further, effect of catalyst dosages were observed by varying the amount the catalyst in the solution. An amount of 0.1 g, 0.2 g, 0.4 g, 0.6 g, were added in separate photocatalytic experiment. The higher activity was observed when 0.4 g catalyst was added and further addition the catalyst dose i.e. 0.6 g, the photocatalytic activity was decrease as shown in Fig. 8b. The higher dosage of the catalyst create turbidity in the solution which reduced the penetration of light to the active sites. Furthermore, the particle agglomeration and enhanced recombination of photogenerated electron-hole pairs reduce the formation of ROS thereby lowering the photocatalytic activity. Therefore, from the results, the optimum catalyst dosage for the better photocatalytic activity was found to be 0.4 g of the $CoFe_2O_4$ nanoparticle. The durability of the $CoFe_2O_4$ nanoparticle was also studies through the recycling experiment. Post each photocatalytic run, $CoFe_2O_4$ was recovered, centrifuged, washed several times with deionised water and acetone to remove any impurity for reuse in four more consecutive degradation experiments. The photocatalytic efficiency of $CoFe_2O_4$ dropped by only (2.4%) after four repeated uses, verifying its high stability and recyclability as shown in Fig. 8c. In addition, to verify the role of reactive oxygen species (ROS), various trapping agents of 1 mM were added during the photocatalytic process. Interestingly, when IPA was introduced, a significant change in the rate constant was obtained and minimal change was observed when Na-EDTA and p-benzoquinone was introduced as shown in Fig. 8d. Therefore it can be concluded that hydroxyl radicals (°OH) is found to be the main reactive species for the degradation of MB dye, however, h+ and $°O_2^-$ are also accountable for the photodegradation of MB dye but their contribution is comparatively less.

3.5. Antibacterial activity evaluation

The $CoFe_2O_4$ antibacterial efficiency was studied using a set of Gram-positive and Gram-negative bacterial isolates. The antibacterial activity was performed against *Listeria monocytogenes* (Fig. 9a), *Staphylococcus aureus* (Fig. 9b), *Klebsiella pneumonia* (Fig. 9c), and *Pseudomonas aeruginosa* (Fig. 9d) and the results obtained are ptesented in Table 2.

To assess antibacterial activity, the synthesised nanoparticles were compared with gentamycin a standard commercial antibiotics and the test was performed at 50, 75 and 100 mg/ml, respectively. At concentration 75 mg/ml, the nanoparticles produced an inhibition zone of 15 ± 0.6, 14 ± 06,.01 ± 0.4, 18 ± 02 and 19 ± 0.6 against *Listeria monocytogenes*, *Staphylococcus aureus, Klebsiella pneumoniae,* and *Pseudomonas aeruginosa*.

As illustrated in Fig. 9, the accumulation of nanoparticles within bacterial cells may result in membrane denaturation which in turn influence antibacterial efficiency of the investigated nanostructures. The present findings are in consistent by the study of [36] which reports that $CoFe_2O_4$ NPs exhibit robust activity against gram negative *E.coli* than the against gram positive *S. aureus*. Similarly [37] suggested that these differences arise due to the structural and chemical variation in bacterial cell wall. Additionally this study revealed that $CoFe_2O_4$ NPs were considerable less efficient against gram-positive bacteria. In a recent study, $CoFe_2O_4$ NPs synthesized by *Hibiscus rosa-sinensis* extract shows greater sensitivity towards gram negative *E.coli* than towards the gram positive *S.aureus*. For better understanding of the antibacterial mechanism of $CoFe_2O_4$ nanoparticles against bacteria, leading to the cell membrane damage and cell death, a probable mechanism is illustrated in Fig. 10.

Based on the results obtained from this study, a comparative table (Table S2) have been provided in the supplementry information, summarizing the bandgap energy, degradation efficiency, rate constant and antibacterial performance of $CoFe_2O_4$.

4. Conclusion

To conclude, MB dye has been effectively adsorbed on the surface $CoFe_2O_4$ nanoparticles and degraded by photocatalytic process. An excellent photocatalytic activity of $CoFe_2O_4$ was obtained i.e. 94.7% towards MB dye is attributed to the lower recombination rate of electron-hole pairs and the formation of reactive oxygen species. The $CoFe_2O_4$ was found stable even after four consecutive cycle of the photodegradation which was confirmed through the recycling experiment. Further, $CoFe_2O_4$ has shown excellent zone of inhibition toward all bacterial starin. Maximum zone of inhibition was shown towards *Klebsiella pneumoniae* strain at 100 mg/ml of concentration. Overall, $CoFe_2O_4$ has demonstrated a dual role i.e. in the antibacterial activity and photodegradation of MB due to its excellent redox property, surface

area and adsorption capacity. The further research could be focused on the reusability and the implementation of the photocatalyst for the real wastewater applications and for the biomedical applications.

CRediT authorship contribution statement

Sabeeha Jabeen: Methodology, Writing – original draft. **Nafees Ahmad:** Conceptualization, Supervision, Validation, Writing – review & editing. **Naseem Ahmad:** Formal analysis, Investigation, Methodology. **Vasi Uddin Siddiqui:** Investigation, Visualization. **Shumaila Suhail:** Conceptualization, Data curation, Methodology, Visualization. **Arshad Iqbal:** Data curation, Investigation. **Sana Nisar:** Formal analysis, Methodology, Writing – original draft.

Declaration of Competing Interest

The authors declare that they have no known competing financial interests or personal relationships that could have appeared to influence the work reported in this paper.

Acknowledgments

The authors gratefully acknowledge Integral University, Lucknow, India, for providing the necessary facilities and also thankful to Dean, Research & Development for providing manuscript communication number (IU/R&D/2026-MNC0004401).

Appendix A. Supporting information

Supplementary data associated with this article can be found in the online version at doi:10.1016/j.nxmate.2026.102045.

References

[1] M. Amiri, M. Salavati-Niasari, A. Akbari, Magnetic nanocarriers: evolution of spinel ferrites for medical applications, Adv. Colloid Interface Sci. 265 (2019) 29–44.
[2] S. Jabeen, V.U. Siddiqui, S. Sharma, S. Rai, P. Bansal, S. Bala, T. Khan, A novel green synthesis of $CuFe_2O_4$ Nanoparticles from Cissus rotundifolia for photocatalytic and antimicrobial activity evaluation, J. Alloy. Compd. 984 (2024) 174020.
[3] D. Varshney, K. Verma, Substitutional effect on structural and dielectric properties of Ni1− xAxFe2O4 (A= Mg, Zn) mixed spinel ferrites, Mater. Chem. Phys. 140 (1) (2013) 412–418.
[4] S.J. Salih, W.M. Mahmood, Review on magnetic spinel ferrite (MFe2O4) nanoparticles: from synthesis to application, Heliyon 9 (6) (2023).
[5] B. Bhaduri, A.K. Dikshit, T. Kim, K.M. Tripathi, Research progress and prospects of spinel ferrite nanostructures for the removal of nitroaromatics from wastewater, ACS Appl. Nano Mater. 5 (11) (2022) 16000–16026.
[6] K.K. Kefeni, B.B. Mamba, T.A. Msagati, Application of spinel ferrite nanoparticles in water and wastewater treatment: a review, Sep. Purif. Technol. 188 (2017) 399–422.
[7] E.H. Khader, S.A. Muslim, N.M.C. Saady, N.S. Ali, I.K. Salih, T.J. Mohammed, S. Zendehboudi, Recent advances in photocatalytic advanced oxidation processes for organic compound degradation: a review, Desalin. Water Treat. 318 (2024) 100384.
[8] A. Iqbal, T. Ahamad, F.A. Qais, N. Ahmad, A. Shafi, A.S. Ahmed, S. Srivastava, Proficient visible-light-driven photocatalytic and anti-biofilm activity of biosynthesized CeO2-graphene oxide nanocomposites, Mater. Chem. Phys. 298 (2023) 127397.
[9] N. Ahmad, S. Sultana, A. Azam, S. Sabir, M.Z. Khan, Novel bio-nanocomposite materials for enhanced biodegradability and photocatalytic activity, N. J. Chem. 41 (18) (2017) 10198–10207.
[10] O.D. Dastjerdi, H. Shokrollahi, S. Mirshekari, A review of synthesis, characterization, and magnetic properties of soft spinel ferrites, Inorg. Chem. Commun. 153 (2023) 110797.
[11] M.W. Alam, N. Dhanda, H.H. Almutairi, N.S. Al-Sowayan, S. Mushtaq, S.A. Ansari, Green ferrites: eco-friendly synthesis to applications in environmental remediation, antimicrobial activity, and catalysis—a comprehensive review, Appl. Organomet. Chem. 39 (2) (2025) e7962.
[12] A.K. Mittal, Y. Chisti, U.C. Banerjee, Synthesis of metallic nanoparticles using plant extracts, Biotechnol. Adv. 31 (2) (2013) 346–356.
[13] J.O. Adeyemi, A.O. Oriola, D.C. Onwudiwe, A.O. Oyedeji, Plant extracts mediated metal-based nanoparticles: synthesis and biological applications, Biomolecules 12 (5) (2022) 627.
[14] K. Arora, L. Ledwani, Komal, A comprehensive review on the synthesis and therapeutic potential of cobalt ferrite (CoFe2O4) nanoparticles, ChemistrySelect 10 (1) (2025) e202404136.
[15] M.N. Kiani, M.S. Butt, I.H. Gul, M. Saleem, M. Irfan, A.H. Baluch, M.A. Raza, Synthesis and characterization of cobalt-doped ferrites for biomedical applications, ACS Omega 8 (4) (2023) 3755–3761.
[16] M. Barani, A. Rahdar, M. Mukhtar, S. Razzaq, M. Qindeel, S.A.H. Olam, S. Pandey, Recent application of cobalt ferrite nanoparticles as a theranostic agent, Mater. Today Chem. 26 (2022) 101131.
[17] K.L. Routray, S. Saha, D. Behera, Green synthesis approach for nano sized CoFe2O4 through Aloe vera mediated sol-gel auto combustion method for high frequency devices, Mater. Chem. Phys. 224 (2019) 29–35.
[18] P. Mahajan, A. Sharma, B. Kaur, N. Goyal, S. Gautam, Green synthesized (Ocimum sanctum and Allium sativum) Ag-doped cobalt ferrite nanoparticles for antibacterial application, Vacuum 161 (2019), 389-39.
[19] N. Kobylinska, D. Klymchuk, A. Shakhovsky, O. Khainakova, Y. Ratushnyak, V. Duplij, N. Matvieieva, Biosynthesis of magnetite and cobalt ferrite nanoparticles using extracts of “hairy” roots: preparation, characterization, estimation for environmental remediation and biological application, RSC Adv. 11 (43) (2021) 26974–26987.
[20] Y. Wang, D. Sun, Q. Jiang, L. Xiong, N. Zhang, Y. Pan, L. Chen, Diterpenoids with anti-inflammatory activity from Euphorbia wallichii, Phytochemistry 205 (2023) 113486.
[21] Sanaz Alamdari, Morteza Sasani Ghamsari, Chan Lee, Wooje Han, Hyung-Ho Park, Majid Jafar Tafreshi, Hosein Afarideh, Mohammad Hosein Majles Ara, "Preparation and characterization of zinc oxide nanoparticles using leaf extract of Sambucus ebulus, Appl. Sci. 10 (10) (2020) 3620.
[22] S.S. Banifatemi, F. Davar, B. Aghabarari, J.A. Segura, F.J. Alonso, S.M. Ghoreishi, Green synthesis of CoFe2O4 nanoparticles using olive leaf extract and characterization of their magnetic properties, Ceram. Int. 47 (13) (2021) 19198–19204.
[23] K. Kombaiah, J.J. Vijaya, L.J. Kennedy, M. Bououdina, R.J. Ramalingam, H.A. Al-Lohedan, Comparative investigation on the structural, morphological, optical, and magnetic properties of CoFe2O4 nanoparticles, Ceram. Int. 43 (10) (2017) 7682–7689.
[24] Y. Oh, M. Sahu, S. Hajra, A.M. Padhan, S. Panda, H.J. Kim, Spinel ferrites (CoFe2O4): synthesis, magnetic properties, and electromagnetic generator for vibration energy harvesting: Y. Oh, M. Sahu et al, J. Electron. Mater. 51 (5) (2022) 1933–1939.
[25] S.M. Matar, G.H. Ramzy, M. Arif, I.M. Maafa, A. Yousef, N. Zouli, A. Ali, Chemical synthesis of Nd x Co 1− x Fe 2 O 4 hybrid nanoparticles for permanent magnet applications: structural, magnetic and electrical properties, Nanoscale Adv. 7 (9) (2025) 2725–2741.
[26] M.N. Rashin, J. Hemalatha, Magnetic and ultrasonic studies on stable cobalt ferrite magnetic nanofluid, Ultrasonics 54 (3) (2014) 834–840.
[27] P. Seeharaj, P. Pasupong, K. Choojun, Magnetically separable CeO2/CoFe2O4 heterojunction photocatalysts for dye degradation: characterization and mechanism, J. Asian Ceram. Soc. 12 (1) (2024) 44–58.
[28] H. Hussein, S.S. Ibrahim, S.A. Khairy, Biosynthesis of CoFe2O4 ferrite nanoparticles using Greek yogurt solution: Deep structural insights and appraisal for ecological mitigation via quartz crystal microbalance, J. Water Process Eng. 65 (2024) 105856.
[29] M. Saquib, A. Halder, Dealloyed Pt3Co nanoparticles with higher geometric strain for superior hydrogen evolution reaction, J. Solid State Chem. 262 (2018) 229–236.
[30] N. Ahmad, S. Sultana, S.M. Faisal, A. Ahmed, S. Sabir, M.Z. Khan, Zinc oxide-decorated polypyrrole/chitosan bionanocomposites with enhanced photocatalytic, antibacterial and anticancer performance, RSC Adv. 9 (70) (2019) 41135–41150.
[31] A. Rai, A.K. Thakur, Co-substitution tailored dielectric relaxation and electrical conduction in lanthanum orthoferrite, Ceram. Int. 46 (14) (2020) 22752–22765.
[32] S. Jabeen, A.S. Ganie, N. Ahmad, S. Hijazi, S. Bala, D. Bano, T. Khan, Fabrication and studies of LaFe2O3/Sb2O3 heterojunction for enhanced degradation of Malachite green dye under visible light irradiation, Inorg. Chem. Commun. 152 (2023) 110729.
[33] A. Shafi, N. Ahmad, S. Sultana, S. Sabir, M.Z. Khan, Ag_2S-sensitized NiO–ZnO heterostructures with enhanced visible light photocatalytic activity and acetone sensing property, ACS Omega 4 (7) (2019) 12905–12918.
[34] N. Ahmad, G. Kumar, I.H. Faridi, R.S. Dey, Synergistic ternary polypyrrole/WO 3/MWCNT nanocomposites for environmental remediation and electrochemical water splitting, Dalton Trans. 55 (9) (2026) 3814–3827.
[35] N. Ahmad, J. Anae, M.Z. Khan, S. Sabir, P. Campo, F. Coulon, A novel CuBi2O4/polyaniline composite as an efficient photocatalyst for ammonia degradation, Heliyon 8 (8) (2022).
[36] N. Sanpo, C.C. Berndt, C. Wen, J. Wang, Transition metal-substituted cobalt ferrite nanoparticles for biomedical applications, Acta Biomater. 9 (3) (2013) 5830–5837, https://doi.org/10.1016/j.actbio.2012.10.037.
[37] A. Nahar, K.H. Maria, S.I. Liba, M. Anwaruzzaman, M.N. Khan, A. Islam, et al., Surface-modified CoFe2O4 nanoparticles using folate-chitosan for cytotoxicity studies, hyperthermia applications and positive/negative contrast of MRI, J. Magn. Magn. Mater. 554 (2022) 169282, https://doi.org/10.1016/j.jmmm.2022.169282.